BIOCHEMISTRY
including biophysical chemistry & molecular biology

Article

pubs.acs.org/biochemistry

Models for the Metal Transfer Complex of the N-Terminal Region of CusB and CusF

Melek N. Ucisik,[†,‡] Dhruva K. Chakravorty,[§] and Kenneth M. Merz, Jr.*[,∥]

[†]Department of Chemistry and Quantum Theory Project, University of Florida, 2328 New Physics Building, P.O. Box 118435, Gainesville, Florida 32611-8435, United States

[‡]Department of Chemistry, University of Illinois at Urbana-Champaign, 600 South Mathews Avenue, Urbana, Illinois 61801-3364, United States

[§]Department of Chemistry, University of New Orleans, 2000 Lake Shore Drive, New Orleans, Louisiana 70148, United States

[∥]Institute for Cyber Enabled Research, Department of Chemistry, and Department of Biochemistry and Molecular Biology, Michigan State University, 578 South Shaw Lane, East Lansing, Michigan 48824-1322, United States

Supporting Information

ABSTRACT: The tripartite CusCFBA pump in *Escherichia coli* is a very effective heavy metal extrusion system specific for Cu(I) and Ag(I). The N-terminal region of the membrane fusion protein CusB (CusB-NT) is highly disordered, and hence, experimentally characterizing its structure is challenging. In a previous study, this disorder was confirmed with molecular dynamics simulations, although some key structural elements were determined. It was experimentally shown that CusB-NT is fully functional in transferring the metal from the metallochaperone CusF. In this study, we docked these two entities together and formed two representative metal coordination modes, which consist of residues from both proteins. In this way, we created two potential CusB-NT/CusF complexes that share coordination of Cu(I) and thereby represent structural models for the metal transfer process. Each model complex was simulated for 4 μs. The previously observed structural disorder in CusB-NT disappeared upon complexation with CusF. The only differences between the two models occurred in the M21−M36 loop region of CusB-NT and the open flap of CusF: we observed the model with two CusB-NT methionine residues and a CusF methionine as the metal coordination site (termed "MMM") to be more stable than the model with a CusB-NT methionine, a CusF methionine, and a CusF histidine ligating the metal (termed "MMH"). The observed stability of the MMM model was probed for an additional 2 μs, yielding a total simulation time of 6 μs. We hypothesize that both MMM and MMH configurations might take part in the metal exchange process in which the MMH configuration would appear first and would be followed by the MMM configuration. Given the experimental finding of comparable binding affinities of CusB-NT and CusF, the increased stability of the MMM configuration might be a determinant for the transfer from CusF to CusB-NT. The metal would be transferred from the more CusF-dominated metal binding environment (MMH model) to a more CusB-dominated one (MMM model) in which the coordination environment is more stable. From the MMM model, the metal ion would ultimately be coordinated by the CusB methionines only, which would complete the Cu(I) transfer process.

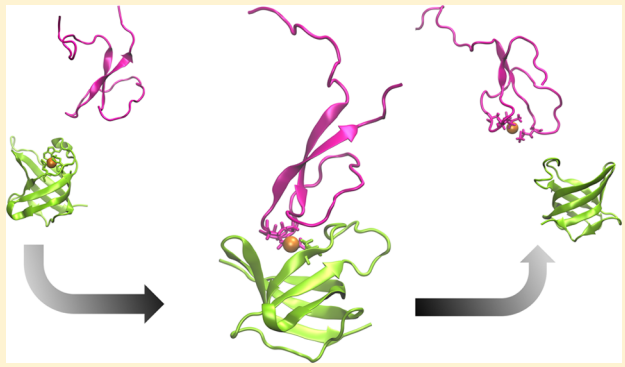

The CusCFBA efflux system in *Escherichia coli* expels Cu(I) and Ag(I) when the concentrations of these heavy metals reach lethal levels within the cell. It comprises CusA, the inner membrane proton/substrate antiporter of the heavy metal efflux-RND family, CusB, the periplasmic protein, and CusC, the outer membrane protein.[1−3] The Cus system is completed by an additional fourth component, CusF, which serves as a periplasmic Cu(I)/Ag(I) metallochaperone and is crucial for maximal metal resistance.[2,4] The periplasmic protein CusB belongs to the membrane fusion protein (MFP) family.[5] It is hypothesized to stabilize the tripartite intermembrane complex by interacting with CusA and CusC. Its available crystal structures resulted in identification of four domains: the membrane proximal, β barrel, lipoyl, and α helical domains. However, its N-terminus, which contains three conserved metal binding Met residues, could not be resolved with crystallographic techniques because it is disordered.[6,7] Recent experiments showed that the N-terminal region of CusB (CusB-NT) is capable of exhibiting metal transfer from CusF by itself, although not as effectively as the full-length CusB, which weakens the hypothesis that CusB behaves simply as a metal

Received: February 24, 2015
Revised: June 1, 2015
Published: June 16, 2015

DOI: 10.1021/acs.biochem.5b00195
Biochemistry 2015, 54, 4226−4235

chelator. A structural change should be induced on the entire CusB chain, which results in higher Cu(I)/Ag(I) resistance by possibly increasing the metal ion transfer rate.[8] Yet the retention of the metal transfer ability by truncated CusB led us to conduct molecular dynamics studies concerning the disordered N-terminal region of CusB that was extracted from the rest of the CusB protein.[9] We found that some structural elements appear repeatedly over the microsecond time frame in both apo and Cu(I)-bound versions of this protein chain, which points to the formation of transient order over this time scale.[9] Additionally, CusB and CusF interact in the presence of metal ion. They display similar metal binding affinities, which was determined from the equal distribution of the metal ion between them when they were mixed in equimolar concentrations *in vitro*.[10,11] Direct metal transfer between these proteins has also been shown experimentally.[12] Chemical cross-linking/mass spectrometry experiments captured the CusB−CusF interaction that highlighted the significance of the N-terminal region in terms of protein−protein interactions and metal transfer.[13,14]

We hypothesize that the metal transfer between CusB and CusF might induce motional restraints on the very mobile N-terminal region of CusB. To explore the structural impacts of this protein−protein interaction, we performed molecular dynamics studies on two models of the CusB-NT/CusF complex bound to Cu(I) ion: the MMM model and the MMH model. In the MMM model, three Met residues ligate the metal, whereas in the MMH model, one of the ligating Met residues is replaced by a His residue. This computational experiment, which involves protein−protein docking followed by extensive MD simulations, also brings us one step closer to our ultimate aim of simulating the metal extrusion process through the CusCFBA pump.

METHODS

The transfer of the Cu(I) ion from the metallochaperone CusF to CusB involves metal ligation sites with contributions from both the CusB and CusF proteins. In CusB, the metal is coordinated by three methionines, M21, M36, and M38,[9] whereas in CusF, the metal site consists of two methionines, M47 and M49, a histidine, H36, and a nonbonded tryptophan, W44, which forms a cation−π contact with the metal ion.[15] During the metal transfer from CusF to CusB, the nonbonded cation−π contact W44 is hypothesized to be the first to break. Hence, we are left with a pool of six residues, three from CusB (M21, M36, and M38) and three from CusF (H36, M47, M49). The transition metal binding sites should involve three-membered combinations of these. This results in 18 potential transfer metal coordination sites, nine of which are dominated by CusF. The remaining nine are dominated by CusB residues. These possibilities are shown in Figure 1. Our docking effort of the open configuration of CusF[16] to CusB-NT yielded two of these potential transfer metal coordination sites as plausible models that could facilitate the transfer of the Cu(I) ion from CusF to CusB. The first model, which we call "MMM", involves a Cu(I) binding site consisting of the Met residues M36 and M38 of CusB-NT and M49 of CusF; thus, it is an example of the CusB-dominated metal binding site models. The second model, "MMH", has the M36 of CusB-NT, the H36 of CusF, and the M49 of CusF bound to Cu(I), representing an example of the CusF-dominated metal binding site models. These potential metal binding sites were based on predictions made by the protein−protein docking server HADDOCK (High

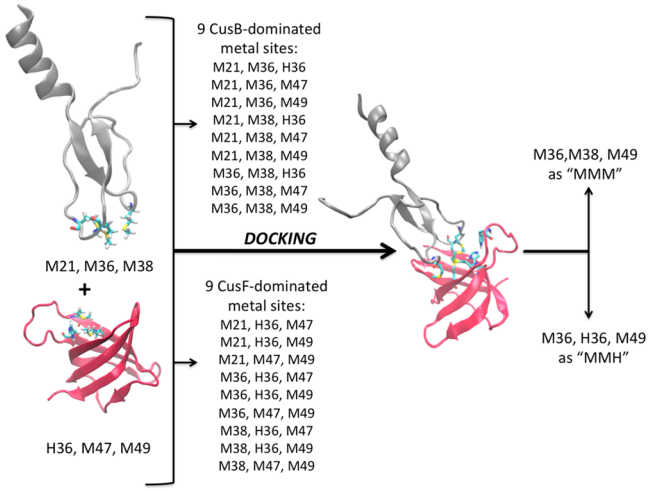

Figure 1. On the left, the N-terminus of CusB and the metallochaperone CusF are shown with their metal binding sites. The metal-ligating residues are listed underneath the structures for each protein. Out of the pool of these six residues, M21, M36, M38, H36, M47, and M49, the possible combinations are listed in the center. Domination by a protein is determined by their contribution to the metal site. Keeping these possible combinations in mind, we docked the two proteins and formed the MMM- and the MMH-bonded metal binding site models based on the positioning of the residues in the top docking hit. This positioning can be seen in Figure 2.

Ambiguity Driven protein−protein DOCKing).[17,18] It presents an information-driven flexible docking approach for the modeling of biomolecular complexes in which it generates models, clusters the generated models, and returns the most populated clusters as docking results. The most populated cluster from HADDOCK docking of Cu(I)-bound CusB-NT[9] with the open conformation of CusF[16] resulted in valid metal transfer environments as shown in Figures 2 and 3.

We introduced the Cu(I) ion into the center of mass of the sulfur atoms of the three Met residues constituting the MMM model (M36 and M38 of CusB-NT and M49 of CusF) and of the two sulfur atoms of the metal binding Met residues in the MMH model along with the ε-nitrogen of the His residue (M36 of CusB-NT, H36 of CusF, and M49 of CusF). The

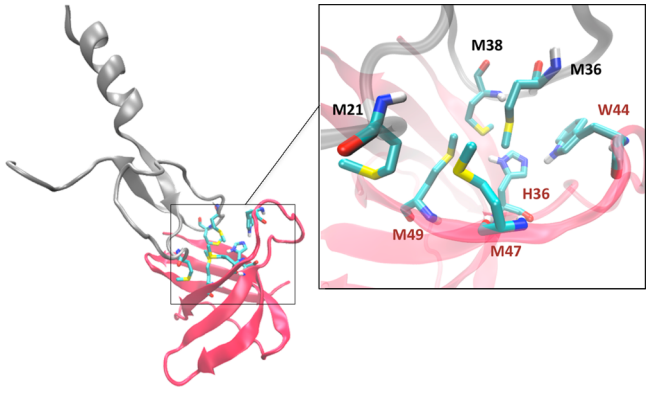

Figure 2. Top hit from the HADDOCK docking of CusB-NT (gray) to the open conformation of CusF (red). The inset shows the positioning of the metal binding residues on CusB (black labels) and CusF (burgundy labels) as they were positioned in the docking pose with the highest score. From this pose, we created the two model mixed binding environments, MMM and MMH.

DOI: 10.1021/acs.biochem.5b00195
Biochemistry 2015, 54, 4226−4235

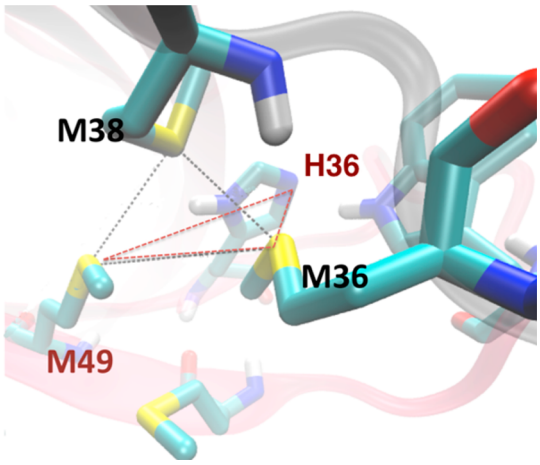

Figure 3. Two model metal binding sites were based on the positioning of the labeled residues. The black triangle shows the initial positions of M36 and M38 of CusB-NT, and M49 of CusF, in the middle of which we introduced Cu(I) to yield the first model binding site, MMM. The metal binding site of the second model, MMH, is comprised of the residues at the corners of the dark red triangle: M36 of CusB-NT and M49 and H36 of CusF. The imidazole ring of H36 was manually rotated so that its NE2 atom faced the sulfur atoms of M36 and M49 before we implemented the Cu(I) ion in their centroid.

needed metal parameters were previously obtained in studies of CusB-NT[9] and CusF[15] using the MTK++/MCPB functionality[19] of AmberTools version 1.5.[20]

In both models, all the protein and solvent atoms were treated explicitly. Each model system was solvated with the TIP3P triangulated water model[21] in a periodically replicated rectangular water box whose sides were at least 10 Å from the solute atoms. The charges of the model systems were neutralized by addition of Na^+ ions, and charged amino acids were modeled in the protonated states obtained with the H++ protonation state server at pH 7.[22] A minimization and equilibration protocol similar to that used in our CusB-NT simulations[9] was employed: an energy minimization series of seven stages involving the minimization of only the solvent atoms and the counterions (stage 1), minimization of the hydrogen atoms (stage 2), minimization of the side chains by gradually decreasing the harmonic positional restraints acting on them (stages 3−6), and finally the energy minimization of the whole system with no positional restraints (stage 7). A total of 53000 energy minimization steps were performed in total, 24000 of which used the steepest descent protocol.[23] The remaining 29000 steps utilized the conjugate gradient method for minimization.[23] A two-stage equilibration protocol followed the minimization. First, the systems were heated slowly from 0 to 300 K over 200 ps of MD within the canonical ensemble (*NVT*) by maintaining a weak harmonic restraint on the protein, and then they were simulated for 10 ns at 300 K to check for the stability of the peptide chains after removal of the harmonic restraints at a constant pressure of 1.0 bar for an isobaric, isothermal ensemble (*NPT*) using Langevin dynamics with a collision frequency of 1.0 ps^{-1}.[24] Periodic boundary conditions were imposed on the systems during the calculation of nonbonded interactions at all minimization and equilibration stages. The lengths of the covalent bonds involving hydrogen were constrained, and their interactions were omitted with the SHAKE algorithm while the systems were heated.[25] All the restraints on the systems were released before we started with the MD production runs. We then ran 4 μs of classical MD using the ff99SBildn force field[26] using the CUDA implementation of the pmemd program in the AMBER12 suite.[27] Throughout the production simulations, the SHAKE algorithm was used to constrain covalent bonds involving hydrogen. The particle mesh Ewald (PME) method was utilized for long-range electrostatic interactions. An 8 Å nonbonded cutoff was applied to limit the direct space sum in PME.[28] The temperature of the systems was kept at 300 K with Langevin dynamics (collision frequency of 1.0 ps^{-1}). Frames were collected every 2 ps. A subset of these snapshots were employed in calculations of the distance, angle, dihedral, root-mean-square deviation (RMSD), and root-mean-square fluctuation (RMSF) with the aid of the ptraj utility in AmberTools version 1.5, and secondary structure assignments were obtained using STRIDE.[29] On the basis of our subsequent observations, we decided to continue the MD simulations on the MMM model for an additional 2 μs with the exact same simulation settings, yielding a total of 6 μs, and we repeated all the described analyses for the entire 6 μs.

RESULTS AND DISCUSSION

In the course of the simulations of the MMM model, the sulfur atoms of M36 and M38 of CusB-NT, M49 of CusF, and the Cu(I) ion presented a distorted tetrahedral geometry with bonds slightly longer than those in the optimized and experimental geometries (by 0.1−0.2 Å on average for both CusB-NT and CusF geometries).[12,30] The sulfur and nitrogen bonding distances in the metal site of the MMH model remained near the optimized distances for the most part, which we obtained through optimization calculations involving methionine and histidine side chains and a Cu(I) ion at the density functional theory (DFT) QM level. These calculations were performed with Gaussian'09[31] using the B3LYP[32] and M06L[33] DFT functionals in conjunction with the double-ζ-quality LANL2DZ pseudopotential basis set for Cu(I)[34] and Pople-type basis set 6-31G* for all the other atoms.[35] The Cu(I) ion and the ligating atoms placed themselves again in a distorted tetrahedron, akin to the MMM case.

Disappearance of Disorder in CusB-NT. The first observation we made on the MMM and MMH models was that this complexation provided the CusB-NT chain with a considerably increased structural stability. Upon visual inspection of the simulations, we observed the β motif in the center of the CusB-NT, which was already present in the starting geometries, was present throughout the trajectory. The tail regions were the most mobile parts akin to the apo and holo noncomplexed CusB-NT MD runs. We assigned secondary structures to snapshots saved from both trajectories using STRIDE. The 400 consecutive frames we employed were separated by 10 ns, yielding a total simulation time of 4 μs. As inferred from visual inspection, the β motif in CusB-NT was always retained and the tails remained mostly disordered, although there was clear formation of an α helix at the N-terminus of the starting CusB-NT structure. The M21−M36 loop was also a random coil. On the CusF side, the largest random coil region proved to be the flap region, namely CusF residues 36−48 (Figure 4), which corresponds to residues 75−87 in cumulative numbering, which was used on the *y*-axis of the STRIDE matrices. Figure 5 displays the disappearance of disorder of the CusB-NT region in both CusB/CusF complex models. The persistence of the β motif is clearly seen in the middle and rightmost panels.

DOI: 10.1021/acs.biochem.5b00195
Biochemistry 2015, 54, 4226−4235

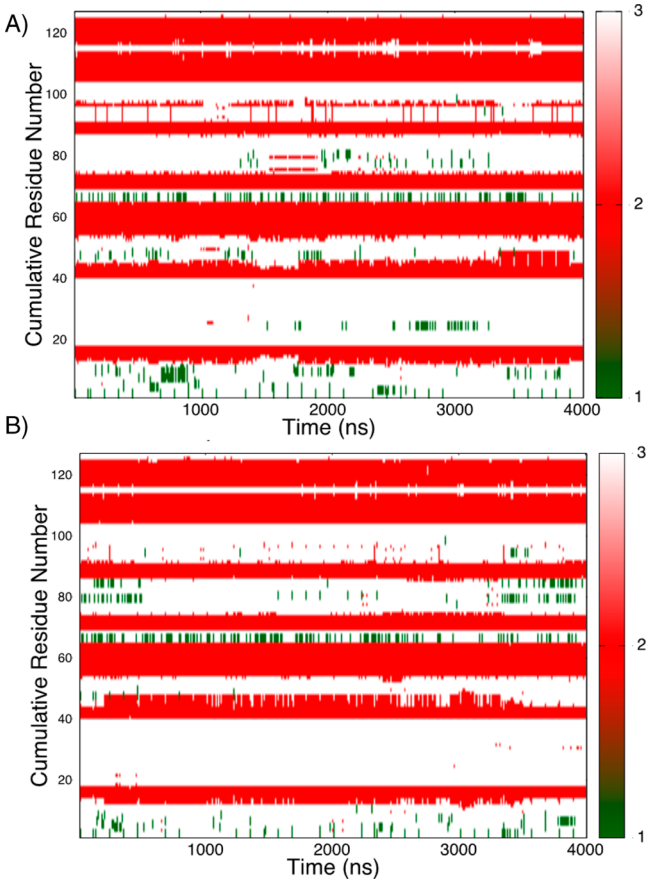

Figure 4. Secondary structure assignments of the CusB-NT/CusF complex for the (A) MMM and (B) MMH models. Residues 1−51 make up CusB-NT, whereas the rest is CusF. Color coding: green, α helix; red, β strand; white, randomly coiled or disordered. The red bands have no interruptions pointing to very consistent β sheets in the entire complex.

MMM versus MMH Models. Over the course of 4 μs of MD simulations, an interesting difference arose between the two models, MMM and MMH. In the MMM model, the very mobile, flap-like M21−M36 loop of CusB-NT interacts with the open flap of CusF, and these two are geometrically "locked" over ∼50% of the simulation time. The interaction appears to be reversible, because we observed the M21−M36 loop and the CusF flap coming together and separating during the course of the simulation. For the metal to be expelled, it must be first fetched by CusF in the periplasm and passed to CusB. This suggests a metal binding site, which first largely involves CusF components, and then a mixture of CusF and CusB components that becomes gradually more dominated by CusB-NT components, and finally only CusB residues. Hence, observing first the MMH model with two constituents from CusF and one constituent from CusB and then switching to the MMM model with one CusF component and two CusB components is a reasonable pathway. In the hypothesized earlier MMH model, the total chain motion slightly exceeds what it is found in the proposed subsequent MMM model. These differ considerably in the extent of motion observed in the M21−M36 loop of CusB-NT, where in the MMH model, this loop and the open flap of CusF move freely and do not strongly interact over 4 μs of simulation time. On the other hand, in the MMM model, an interplay between these two regions noticeably restrains the motions of the CusB-NT M21−M36 loop. This interplay seems to weaken in the additional MD simulations of 2 μs on the MMM model (Supporting Information) with the M21−M36 loop of CusB-NT and the open flap of CusF becoming further separated.

The first analysis we conducted was the comparison of the root-mean-square deviations (RMSD's) of the protein chain backbone atoms in the MMM and MMH models. The first frame of each production run was used as the reference. The average rmsd for the MMM model amounted to 7.40 Å, while for the MMH model, it was 7.83 Å. Hence, the overall structural changes are slightly more pronounced in the MMH model (Figure 6). To check whether these changes were localized or spread along the entire protein complex, we performed a root-mean-square fluctuation (RMSF) analysis, which indicated that the difference in the RMSD's was really a consequence of local mobility in the MMH model. As seen in Figure 7, the mobilities of the two models track each other very well, except for the M21−M36 loop of CusB-NT, which we already observed to interact with the open loop of CusF more strongly in the MMM model. This stronger interaction, which exists in prolonged time frames, stabilizes the loop and renders it less mobile than in the MMH model, which in turn gives rise to higher rmsd values for the MMH model. Taking the rmsd and rmsf analyses from the additional 2 μs of simulation time for the MMM model into account, we see that the overall

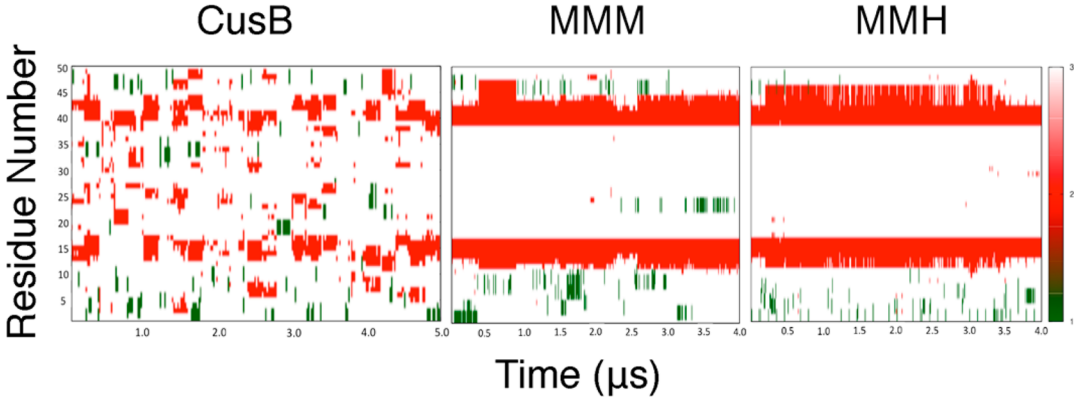

Figure 5. Stride assignments for CusB-NT alone (left) and CusB-NT complexed with CusF, the MMM model (center), and the MMH model (right). The central β strand motif persists in the complexed models at all times as a sign of how the disorder of CusB-NT disappeared upon complexation.

DOI: 10.1021/acs.biochem.5b00195
Biochemistry 2015, 54, 4226−4235

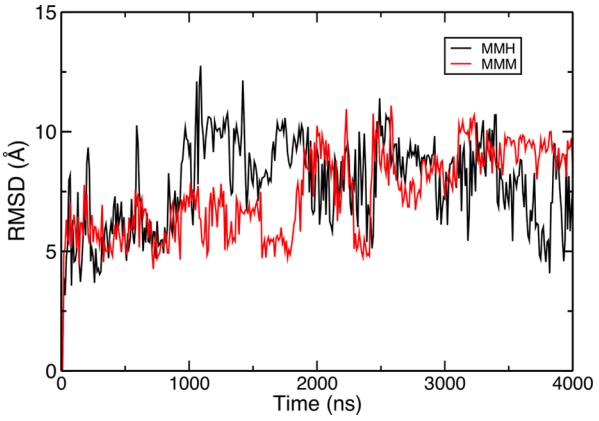

Figure 6. RMSD profiles of the MMM (black) and MMH (red) models over 4 μs of simulation time.

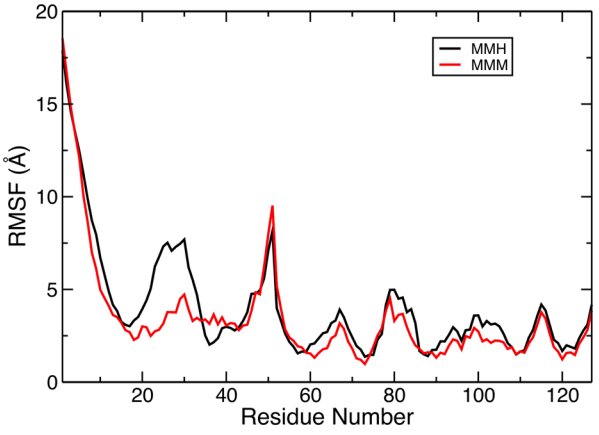

Figure 7. RMSF profiles of the MMM (black) and MMH (red) models over 4 μs of simulation time.

structural stability of this model is enhanced as indicated by the narrower spread of the rmsd fluctuations (Figure S1 of the Supporting Information) and the lower values of the rmsf (Figure S2 of the Supporting Information).

A closer look at the interaction of the M21−M36 loop of CusB and the open flap of CusF was subsequently conducted. We developed various structural coordinates to quantify the properties of this interaction. Visual inspection of the simulation along with the rmsf analysis showed that these two regions of CusB and CusF affect each other significantly because of their proximity. Thus, the first coordinate we used was the distance between the centers of mass of the M21−M36 loop of CusB and the CusF flap. At this point, we should clarify that we consider the residues 36−48 of CusF as the open flap (75−87 in the cumulative numbering). We found 10 Å to be the most prevalent value for this distance in the MMM model, whereas in the MMH model, it averaged around 20 Å. As a further coordinate, we examined the distance between the α carbon atoms of K32 of CusB and P45 of CusF (position 84 in cumulative numbering). These two residues appear to be especially proximal to each other compared to the centers of mass of the loops, which hints that there might be a stronger interaction between them. In the MMM model, their α carbons are separated by ∼6.0 Å, while in most of the snapshots saved from the MMH run, this separation measures ∼14.0 Å. Figure 8 displays these distances in the course of the simulation, and Figure 9 presents the data in the form of histograms. Both

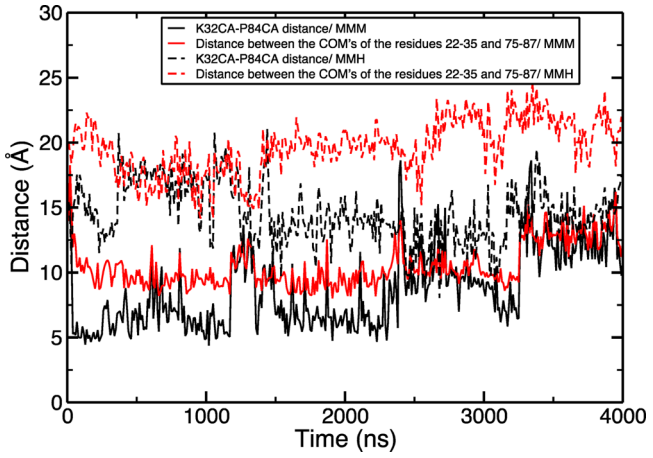

Figure 8. Distances of the M21−M36 loop of CusB-NT and the open flap of CusF expressed in terms of the separation between their centers of mass (red) and the separation between CusB-NT residue K32 and CusF residue P45 (black). Solid lines show the results from the MMM model, and dashed lines represent those from the MMH model. The separation expressed by both of these properties is smaller in the MMM model than in the MMH model.

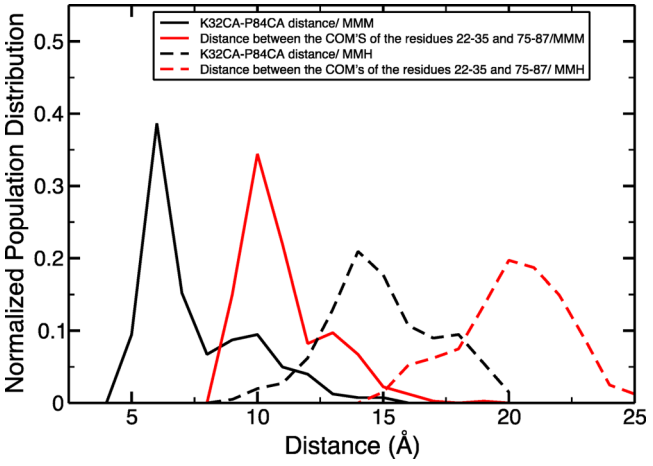

Figure 9. Histograms for the distances of the M21−M36 loop of CusB-NT and the open flap of CusF expressed in terms of the separation between their centers of mass (red) and the separation between CusB-NT residue K32 and CusF residue P45 (black). Solid lines show the results from the MMM model, and dashed lines represent those from the MMH model.

distances converge to similar values in the additional 2 μs of simulation time, and they become larger than what they are in the first 3.5 μs of the simulation, leading to further separation of the M21−M36 loop of CusB-NT and open flap of CusF (Figures S3 and S4 of the Supporting Information).

Closer chains would also correspond to smaller angles of the center of mass of CusB-NT's M21−M36 loop, the Cu(I) ion, and the center of mass of CusF's open flap. Indeed, we probed this angle and saw it was much wider for the MMH model than in the MMM model, in which CusB-NT's loop is found to interact with CusF's flap. In the MMH model, the average value for this property was 93.8° in contrast to 50.9° for the MMM model. Its fluctuations and population densities are shown in Figures 10 and 11. In line with the observations pertaining to the distance between the M21−M36 loop of CusB and the open flap of CusF, these angles increase at ∼3.5 μs into the simulation, which indicates that these two entities are further

DOI: 10.1021/acs.biochem.5b00195
Biochemistry 2015, 54, 4226−4235

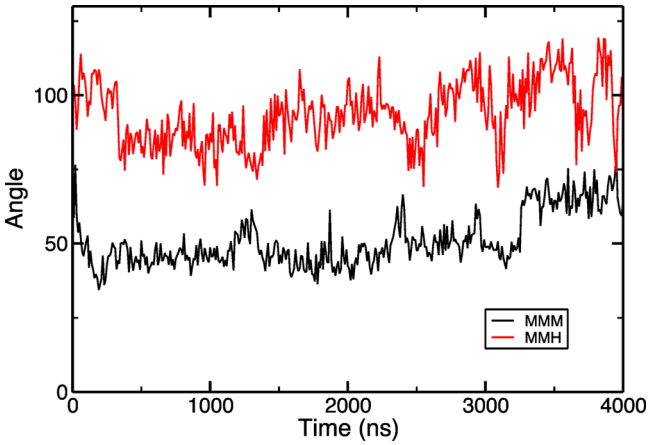

Figure 10. Angle involving the center of mass of CusB-NT's M21−M36 loop, Cu(I), and the center of mass of CusF's open flap over the entire 4 μs production run. Black represents the values from the MMM model and red those from the MMH model.

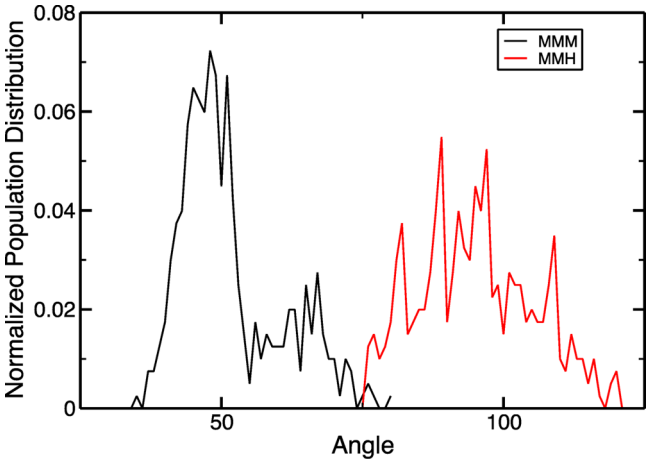

Figure 11. Histograms for the angle involving the center of mass of CusB-NT's M21−M36 loop, Cu(I), and the center of mass of CusF's open flap over the entire production run of 4 μs. Black represents the values from the MMM model and red those from the MMH model.

separating from each other. However, this angle remains still smaller than its counterpart in the MMH model as shown in Figures S5 and S6 of the Supporting Information.

We further analyzed this loop−flap interplay at the level of the molecular interactions present. Previously, we identified a hydrogen bonding network at the "hinge" points of the CusB-NT M21−M36 loop that facilitated its folding against the core of the structure.[9] A detailed visual analysis of likely hydrogen bonding partners on the loop and flap showed some hydrogen bonding occurs between these two, although it is of various types unlike the CusB-NT case. The more consistent hydrogen bonds are formed between one of the guanidinium nitrogens of R26 of CusB-NT and the two side chain oxygen atoms of D46 of CusF, and this sometimes leads to a bifurcated geometry (Figure 12a).[36] In 13% of the saved snapshots, both guanidinium hydrogens of R26 interact with both side chain carboxyl oxygen atoms of D46 to create a salt bridge (Figure 12b). The same salt bridge interactions exist in only 0.02% of the snapshots saved from the MMH simulation. Additionally, weaker hydrogen bonds might also contribute significantly to the loop−flap synergy. The most prominent hydrogen bonds

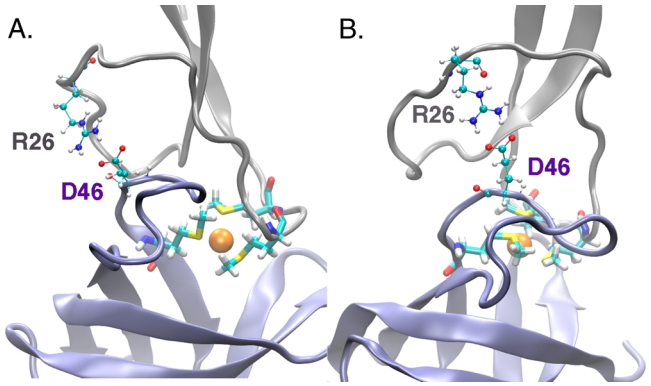

Figure 12. (A) Bifurcated and (B) paired hydrogen bonding interactions between CusB-NT's R26 and CusF's D46. CusB-NT is colored gray and CusF violet.

are observed between the side chain oxygen atom of CusB-NT's Y22 and the backbone nitrogen of CusF's T48. The side chain oxygen of CusB-NT's Y22 switches partners to form another hydrogen bond to the side chain oxygen of CusF's T48, which comes up as the second most common hydrogen bonding interaction. The donor−acceptor distances in these interactions are longer than those associated with the R26−D46 hydrogen bonds, suggesting they are weaker but occur more frequently. They rarely, in only 0.02% of the saved frames, position themselves in a bidentate geometry. As shown in Figure 13, all the corresponding interactions in MMH have distances that are much longer, suggesting very little or no stabilization. The H-bonding network remains mostly unaffected in the additional 2 μs of simulation on the MMM

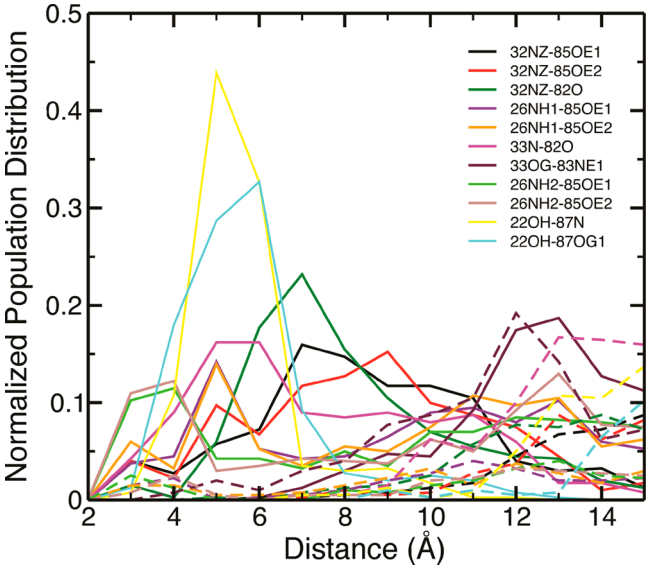

Figure 13. Distances of possible hydrogen bonding partners on the CusB-NT M21−M36 loop and the CusF open flap. Solid lines show the probed distances in the MMM model and the dashed lines those in the MMH model. Involved residues are K32 of CusB-NT ("32"), D46 of CusF ("85"), N43 of CusF ("82"), R26 of CusB-NT ("26"), S33 of CusB-NT ("33"), W44 of CusF ("83"), Y22 of CusB-NT ("22"), and T48 of CusF ("87"). "NZ", "NH1", "NH2", and "NE1" represent side chain nitrogens, while "OE1", "OE2", "OG", and "OH" represent side chain oxygens. "N" is a backbone nitrogen and "O" a backbone oxygen.

DOI: 10.1021/acs.biochem.5b00195
Biochemistry 2015, 54, 4226−4235

model, which might hint at the fact that the tip of the open CusF flap is more mobile than the rest of it. Most of the interaction partners on the CusF side are located toward the end of the flap, so their distances remain mostly constant as seen in Figure S7 of the Supporting Information.

Another factor that might facilitate this geometrical locking of the CusB-NT loop and the CusF flap is the $\pi-\pi$ stacking interaction between the side chains of CusB-NT's F35 and CusF's W44 (83 in cumulative numbering), which actively contributes to metal binding in the closed form of CusF through a π–cation interaction with the cation being either Cu(I) or Ag(I) in this case.[15] We measured the distance between the center of mass of the six carbon atoms making up the phenyl ring of CusB-NT's F35 and the center of mass of six carbon atoms constituting the phenyl part of the indole side chain of CusF's W44. This interaction is observed in both the MMM and MMH models, arising more frequently in the MMM model, which suggests a slightly more favorable interaction. As seen in Figure 14, the most prevalent distance

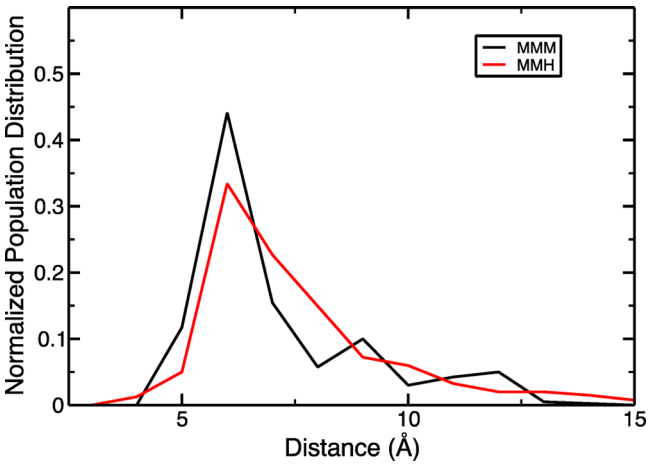

Figure 14. Histograms for the distance between the centroids of the phenyl ring of CusB-NT's F35 and of the phenyl part of the indole ring of CusF's W44. Results for the MMM model are colored black and for the MMH red.

appears at 6 Å for the MMM and MMH models. According to McGaughey et al., distances of <7.5 Å stabilize these conformations energetically;[37] 56% of the snapshots saved from the MMM simulations have values of ≤6 Å, compared to 40% in the MMH simulations. Both parallel and T-shaped conformations occur, as shown in Figure 15. This interaction persists in the additional simulation time of 2 μs on the MMM model. W44 is located between the tip and the hinge of the open flap of CusF, whereas F35 on the CusB-NT side is at the very end of the M21–M36 loop, exactly at the hinge of it, which again results in the observation of the $\pi-\pi$ stacking interaction involving these two residues remaining unchanged over the last 2 μs of the simulation (Figure S8 of the Supporting Information).

CONCLUSIONS

The study focused on the dynamics of the two proposed complexes formed by two constituents of the CusCFBA pump, the N-terminal region of the membrane fusion protein CusB, and the metallochaperone CusF. This aggregate is significantly important because it performs a crucial step in the extrusion of metal from the cell in *E. coli*: CusF transfers the metal it fetches

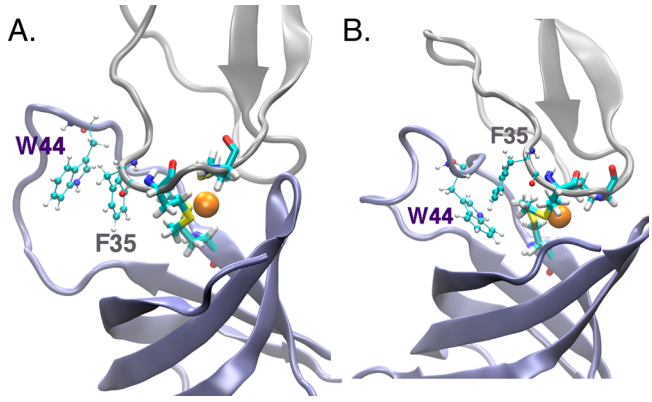

Figure 15. $\pi-\pi$ stacking interaction between the side chains of CusB-NT's F35 and CusF's W44. The common (A) parallel and (B) T-shaped configurations are both observed. CusB-NT is colored gray and CusF violet.

in the periplasm to CusB, which facilitates passing of the metal to CusC to be expelled from the cell. The N-terminal region of CusB contains the metal binding site and was found to be so disordered that its structure could not be resolved spectroscopically. The general disorder was also confirmed by our earlier MD studies, although some key secondary structures were observed.[9] However, the assembly of the N-terminal region of the CusB and CusF presents an interesting case in which the order in the β barrel protein CusF seems to be embraced by the originally disordered CusB-NT. The secondary structures, which were present in the starting geometries, were retained throughout the MD simulations, namely in two parallel runs of 4 μs each. This is not new for CusF but definitely a significant observation for CusB-NT in terms of its overall stability. The observed relative "order" was preserved in the extended MD run on one of the proposed CusB-NT/CusF complex models for an additional 2 μs.

The complex structures were obtained by docking the protein chain of holo CusB to the open conformation of CusF[16] using the protein–protein docking web server HADDOCK (high-ambiguity-driven protein–protein docking). The docking pose with the best score positioned the metal binding residues of both CusB and CusF in an appropriate manner through which we built two model Cu(I) binding sites. The first model-built binding site employed M36 and M38 from CusB-NT and M49 from CusF, which more closely resembles the metal site of CusB. The second model-built binding site was similar to that of CusF that involves two Met residues (M36 of CusB and M49 of CusF) and one His residue (H36 of CusF). Classical 4 μs MD simulations on each model resulted in differences in the mobility of CusB-NT's M21–M36 loop and CusF's open flap. In the model in which the Cu(I) ion is ligated with the three Met residues, the M21–M36 loop of CusB-NT and the open flap of CusF interact over most of the simulation time and become geometrically locked with each other, which in turn decreases the extent of their motion. In contrast, the model in which two Met residues and one His residue coordinate the Cu(I) ion shows greater mobility in CusB-NT's M21–M36 loop and CusF's open flap. The M21–M36 loop of CusB-NT and the open flap of CusF might stay together as a result of a hydrogen bonding network and $\pi-\pi$ stacking interactions. The hydrogen bonding network utilizes various types of hydrogen bonds, including salt bridges (bifurcated) and paired ones. More abundant are the weaker

DOI: 10.1021/acs.biochem.5b00195
Biochemistry 2015, 54, 4226–4235

hydrogen bonds that place the donor and acceptor atoms at distances of >3 Å. A $\pi-\pi$ stacking interaction is proposed also to play a role in stabilizing this interaction. It is the most abundant interaction between these two regions and is found in both models, although it is more common in the model involving three Met residues in its metal site. To further investigate the locking of the M21−M36 loop of CusB-NT and the open loop of CusF, the MD simulation on the MMM model was continued for an additional 2 μs. The loop and the flap further separated from one another as indicated by the loop distances and angles. The impact of this modest separation is not really felt by the hydrogen bonding network and the $\pi-\pi$ stacking interactions because the interaction partners are mostly placed toward the hinge of these entities and not the tips. The tips appear to be more mobile on both the M21−M36 loop of CusB-NT and the open flap of CusF. Even after the separation of the loop and the flap, the distances and angles are still wider in the model with the metal site dominated by the CusF residues compared to that in which the metal ligation site is dominated by CusB residues.

All these observations led us to hypothesize that both models might occur in order: first the model with two methionines and one histidine and then the model with three methionines we hypothesize represent steps of the metal transfer process. This suggests a metal coordination site, which is gradually dominated by CusB residues and is slightly more ordered. The observed stability in the rest of the CusB-NT chain is already surprising when in complex with CusF. Some transient order for the CusB-NT seems likely while CusF delivers the metal to CusB (or vice versa) so that the two proteins align themselves around the metal and exchange the metal ion successfully. The proposed sequence for the transition metal site geometries likely promotes the transfer of metal from CusF to CusB by following an increased structural order in the course of the transfer. Although directionality is not a must for the CusF−CusB interaction, because it was experimentally shown to be rapid and reversible,[8,12] the urgency of the lethal concentrations of Ag(I) and Cu(I) to be alleviated by the Cus system might slightly favor the transfer from CusF to CusB, which was proposed to switch the entire pump to efficient extrusion mode.[14] The gained transient order in the model with three metal-coordinating methionines could be a driving force for the direction of the metal transfer once the pump is turned on by metal transfer from CusF to CusB: toward the extracellular milieu through CusF, CusA, and then CusC. Considering the experimental finding in which the metal gets distributed evenly among CusB-NT and CusF when introduced into a solution containing equal amounts of these proteins, which implies similar metal binding affinities for CusB and CusF, gaining a higher extent of order during the metal transfer process might contribute to determining which direction the metal ion is moved. In this case, the model providing more order is dominated by CusB residues and resembles the metal environment of CusB with its three methionines. To complete the transfer from CusF to CusB-NT would then proceed from the MMM case to the full CusB-NT coordinated mode where CusF's M49 would be replaced by CusB-NT's M21. These two residues are very proximal to each other already in the MMM model, facilitating this final transfer step. Nevertheless, the favorability of the MMM model due to its higher transient order compared to that of the MMH model might be small enough to be overcome by the equilibrium involving the apo version of CusF and the holo version of CusB-NT, and thus, the proposed sequence above could be reversed to permit back transfer from CusB to CusF. That is, if the periplasmic concentration of Ag(I) or Cu(I) decreases to the levels required for homeostasis, the metal ions bound to CusB-NT pieces can still be transferred from CusB-NT to CusF via first the MMM and then the MMH models to switch the Cus pump off.

The fact that we observed some loss of this strong loop−flap interaction between CusB-NT and CusF in the first metal ligation model hints at two possible hypotheses. (1) This 6 μs span of MD simulation insufficiently samples this complex. Even with the observed separation, the first metal ligation model preserves a more pronounced interplay between the loop and the flap along with an overall more stable CusB-NT/CusF complex. (2) These transient metal binding complexes during the metal transfer process from CusF to CusB might have extremely short life spans, and hence, the simulation time of 3.5−4 μs might actually cover the actual lifetime of these interactions.

It is important to note that these simulations supported our initial hypothesis, about the possible disappearance of disorder in CusB-NT upon its complexation with its functional companion, CusF. This work has provided deeper insight into the process of the transfer of metal from CusF to CusB along with other metal transfer processes involving disordered protein chains.

■ ASSOCIATED CONTENT

Supporting Information

Analysis plots for 6 μs of MD data for the MMM model. The Supporting Information is available free of charge on the ACS Publications website at DOI: 10.1021/acs.biochem.5b00195.

■ AUTHOR INFORMATION

Corresponding Author

*E-mail: kmerz1@gmail.com. Phone: (517) 884-2540. Fax: (517) 353-7248.

Funding

We gratefully acknowledge the National Institutes of Health (K.M.M., GM044974) and the National Science Foundation (D.K.C., NSF-EPSCoR LASiGMA EPS-1003897) for funding this project and are thankful for the high-performance computing at the University of Florida and Louisiana Optical Network Initiative for their support.

Notes

The authors declare no competing financial interest.

■ ABBREVIATIONS

MMM, methionine-methionine-methionine; MMH, methionine-methionine-histidine; RND, resistance-nodulation-division; MFP, membrane fusion protein; CusB-NT, CusB N-terminus; HADDOCK, high-ambiguity-driven protein−protein docking; AMBER, Assisted Model Building with Energy Refinement; TIP3P, transferable intermolecular potential 3P; MD, molecular dynamics; *NVT* ensemble, canonical ensemble; *NPT* ensemble, isobaric−isothermal ensemble; PME, particle mesh Ewald; DFT, density functional theory; MCPB, metal center parameter builder; rmsd, root-mean-square deviation; rmsf, root-mean-square fluctuation; STRIDE, structural identification; VMD, visual molecular dynamics.

DOI: 10.1021/acs.biochem.5b00195
Biochemistry 2015, 54, 4226−4235

REFERENCES

(1) Franke, S., Grass, G., and Nies, D. H. (2001) The product of the ybdE gene of the *Escherichia coli* chromosome is involved in detoxification of silver ions. *Microbiology (London, U.K.) 147*, 965−972.

(2) Franke, S., Grass, G., Rensing, C., and Nies, D. H. (2003) Molecular analysis of the copper-transporting efflux system CusCFBA of *Escherichia coli*. *J. Bacteriol. 185*, 3804−3812.

(3) Munson, G. P., Lam, D. L., Outten, F. W., and O'Halloran, T. V. (2000) Identification of a copper-responsive two-component system on the chromosome of *Escherichia coli* K-12. *J. Bacteriol. 182*, 5864−5871.

(4) Loftin, I. R., Franke, S., Roberts, S. A., Weichsel, A., Heroux, A., Montfort, W. R., Rensing, C., and McEvoy, M. M. (2005) A novel copper-binding fold for the periplasmic copper resistance protein CusF. *Biochemistry 44*, 10533−10540.

(5) Saier, M. H., Tam, R., Reizer, A., and Reizer, J. (1994) 2 Novel Families of Bacterial-Membrane Proteins Concerned with Nodulation, Cell-Division and Transport. *Mol. Microbiol. 11*, 841−847.

(6) Su, C. C., Long, F., Zimmermann, M. T., Rajashankar, K. R., Jernigan, R. L., and Yu, E. W. (2011) Crystal structure of the CusBA heavy-metal efflux complex of *Escherichia coli*. *Nature 470*, 558−562.

(7) Su, C. C., Yang, F., Long, F., Reyon, D., Routh, M. D., Kuo, D. W., Mokhtari, A. K., Van Ornam, J. D., Rabe, K. L., Hoy, J. A., Lee, Y. J., Rajashankar, K. R., and Yu, E. W. (2009) Crystal Structure of the Membrane Fusion Protein CusB from *Escherichia coli*. *J. Mol. Biol. 393*, 342−355.

(8) Mealman, T. D., Zhou, M. W., Affandi, T., Chacon, K. N., Aranguren, M. E., Blackburn, N. J., Wysocki, V. H., and McEvoy, M. M. (2012) N-Terminal Region of CusB Is Sufficient for Metal Binding and Metal Transfer with the Metallochaperone CusF. *Biochemistry 51*, 6767−6775.

(9) Ucisik, M. N., Chakravorty, D. K., and Merz, K. M. (2013) Structure and Dynamics of the N-Terminal Domain of the Cu(I) Binding Protein CusB. *Biochemistry 52*, 6911−6923.

(10) Bagai, I., Liu, W., Rensing, C., Blackburn, N. J., and McEvoy, M. M. (2007) Substrate-linked conformational change in the periplasmic component of a Cu(I)/Ag(I) efflux system. *J. Biol. Chem. 282*, 35695−35702.

(11) Kittleson, J. T., Loftin, I. R., Hausrath, A. C., Engelhardt, K. P., Rensing, C., and McEvoy, M. M. (2006) Periplasmic metal-resistance protein CusF exhibits high affinity and specificity for both Cu-I and Ag-I. *Biochemistry 45*, 11096−11102.

(12) Bagai, I., Rensing, C., Blackburn, N. J., and McEvoy, M. M. (2008) Direct Metal Transfer between Periplasmic Proteins Identifies a Bacterial Copper Chaperone. *Biochemistry 47*, 11408−11414.

(13) Mealman, T. D., Bagai, I., Singh, P., Goodlett, D. R., Rensing, C., Zhou, H., Wysocki, V. H., and McEvoy, M. M. (2011) Interactions between CusF and CusB Identified by NMR Spectroscopy and Chemical Cross-Linking Coupled to Mass Spectrometry. *Biochemistry 50*, 2559−2566.

(14) Chacon, K. N., Mealman, T. D., McEvoy, M. M., and Blackburn, N. J. (2014) Tracking metal ions through a Cu/Ag efflux pump assigns the functional roles of the periplasmic proteins. *Proc. Natl. Acad. Sci. U.S.A. 111*, 15373−15378.

(15) Chakravorty, D. K., Wang, B., Ucisik, M. N., and Merz, K. M. (2011) Insight into the Cation-π Interaction at the Metal Binding Site of the Copper Metallochaperone CusF. *J. Am. Chem. Soc. 133*, 19330−19333.

(16) Chakravorty, D. K., Li, P., Tran, T. T., Bayse, C. A., and Merz, K. M. (2015) Metal Capture Mechanism of a Copper Metallochaperone, *J. Am. Chem. Soc.*, submitted for publication.

(17) Dominguez, C., Boelens, R., and Bonvin, A. M. J. J. (2003) HADDOCK: A protein-protein docking approach based on biochemical or biophysical information. *J. Am. Chem. Soc. 125*, 1731−1737.

(18) De Vries, S. J., van Dijk, A. D. J., Krzeminski, M., van Dijk, M., Thureau, A., Hsu, V., Wassenaar, T., and Bonvin, A. M. J. J. (2007) HADDOCK versus HADDOCK: New features and performance of HADDOCK2.0 on the CAPRI targets. *Proteins: Struct., Funct., Bioinf. 69*, 726−733.

(19) Peters, M. B., Yang, Y., Wang, B., Fusti-Molnar, L., Weaver, M. N., and Merz, K. M. (2010) Structural Survey of Zinc-Containing Proteins and Development of the Zinc AMBER Force Field (ZAFF). *J. Chem. Theory Comput. 6*, 2935−2947.

(20) Case, D. A., Darden, T. A., Cheatham, T. E., III, Simmerling, C. L., Wang, J., Duke, R. E., Luo, R., Walker, R. C., Zhang, W., Merz, K. M., Roberts, B., Wang, B., Hayik, S., Roitberg, A., Seabra, G., Kolossvai, I., Wong, K. F., Paesani, F., Vanicek, J., Liu, J., Wu, X., Brozell, S. R., Steinbrecher, T., Gohlke, H., Cai, Q., Ye, X., Wang, J., Hsieh, M.-J., Cui, G., Roe, D. R., Mathews, D. H., Seetin, M. G., Sagui, C., Babin, V., Luchko, T., Gusarov, S., Kovalenko, A., and Kollman, P. A. (2010) *AMBER 11*, University of California, San Francisco.

(21) Jorgensen, W. L., Chandrasekhar, J., Madura, J. D., Impey, R. W., and Klein, M. L. (1983) Comparison of Simple Potential Functions for Simulating Liquid Water. *J. Chem. Phys. 79*, 926−935.

(22) Gordon, J. C., Myers, J. B., Folta, T., Shoja, V., Heath, L. S., and Onufriev, A. (2005) H++: A server for estimating pK_as and adding missing hydrogens to macromolecules. *Nucleic Acids Res. 33*, W368−W371.

(23) Leach, A. R. (2001) *Molecular Modelling: Principles and Applications*, 2nd ed., Pearson Education Ltd., Essex, U.K.

(24) Allen, M. P., and Tildesley, D. J. (1987) *Computer Simulations of Liquids*, Clarendon Press, Oxford, U.K.

(25) Ryckaert, J. P., Ciccotti, G., and Berendsen, H. J. C. (1977) Numerical integration of the cartesian equations of motion of a system with constraints: Molecular dynamics of n-alkanes. *J. Comput. Phys. 23*, 327−341.

(26) Lindorff-Larsen, K., Piana, S., Palmo, K., Maragakis, P., Klepeis, J. L., Dror, R. O., and Shaw, D. E. (2010) Improved side-chain torsion potentials for the Amber ff99SB protein force field. *Proteins: Struct., Funct., Bioinf. 78*, 1950−1958.

(27) Case, D. A., Darden, T. A., Cheatham, T. E., III, Simmerling, C. L., Wang, J., Duke, R. E., Luo, R., Walker, R. C., Zhang, W., Merz, K. M., Roberts, B., Hayik, S., Roitberg, A., Seabra, G., Swails, J., Goetz, A. W., Kolossvai, I., Wong, K. F., Paesani, F., Vanicek, J., Wolf, R. M., Liu, J., Wu, X., Brozell, S. R., Steinbrecher, T., Gohlke, H., Cai, Q., Ye, X., Wang, J., Hsieh, M.-J., Cui, G., Roe, D. R., Mathews, D. H., Seetin, M. G., Salomon-Ferrer, R., Sagui, C., Babin, V., Luchko, T., Gusarov, S., Kovalenko, A., and Kollman, P. A. (2012) *AMBER 12*, University of California, San Francisco.

(28) York, D. M., Darden, T. A., and Pedersen, L. G. (1993) The Effect of Long-Range Electrostatic Interactions in Simulations of Macromolecular Crystals: A Comparison of the Ewald and Truncated List Methods. *J. Chem. Phys. 99*, 8345−8348.

(29) Heinig, M., and Frishman, D. (2004) STRIDE: A web server for secondary structure assignment from known atomic coordinates of proteins. *Nucleic Acids Res. 32*, W500−W502.

(30) Kim, E.-H., Rensing, C., and McEvoy, M. M. (2010) Chaperone-mediated copper handling in the periplasm. *Nat. Prod. Rep. 27*, 711−719.

(31) Frisch, M. J., Trucks, G. W., Schlegel, H. B., Scuseria, G. E., Robb, M. A., Cheeseman, J. R., Scalmani, G., Barone, V., Mennucci, B., Petersson, G. A., Nakatsuji, H., Caricato, M., Li, X., Hratchian, H. P., Izmaylov, A. F., Bloino, J., Zheng, G., Sonnenberg, J. L., Hada, M., Ehara, M., Toyota, K., Fukuda, R., Hasegawa, J., Ishida, M., Nakajima, T., Honda, Y., Kitao, O., Nakai, H., Vreven, T., Montgomery, J. A., Jr., Peralta, J. E., Ogliaro, F., Bearpark, M., Heyd, J. J., Brothers, E., Kudin, K. N., Staroverov, V. N., Kobayashi, R., Normand, J., Raghavachari, K., Rendell, A., Burant, J. C., Iyengar, S. S., Tomasi, J., Cossi, M., Rega, N., Millam, N. J., Klene, M., Knox, J. E., Cross, J. B., Bakken, V., Adamo, C., Jaramillo, J., Gomperts, R., Stratmann, R. E., Yazyev, O., Austin, A. J., Cammi, R., Pomelli, C., Ochterski, J. W., Martin, R. L., Morokuma, K., Zakrzewski, V. G., Voth, G. A., Salvador, P., Dannenberg, J. J., Dapprich, S., Daniels, A. D., Farkas, Ö., Foresman, J. B., Ortiz, J. V., Cioslowski, J., and Fox, D. J. (2009) *Gaussian 09*, revision A.02, Gaussian, Inc., Wallingford, CT.

DOI: 10.1021/acs.biochem.5b00195
Biochemistry 2015, 54, 4226−4235

(32) Becke, A. D. (1993) Density-Functional Thermochemistry. 3. The Role of Exact Exchange. *J. Chem. Phys. 98*, 5648−5652.
(33) Zhao, Y., and Truhlar, D. G. (2006) A new local density functional for main-group thermochemistry, transition metal bonding, thermochemical kinetics, and noncovalent interactions. *J. Chem. Phys. 125*, 194101.
(34) Hay, P. J., and Wadt, W. R. (1985) Ab Initio Effective Core Potentials for Molecular Calculations: Potentials for K to Au Including the Outermost Core Orbitals. *J. Chem. Phys. 82*, 299−310.
(35) Ditchfie, R., Hehre, W. J., and Pople, J. A. (1971) Self-consistent molecular-orbital methods. 9. Extended gaussian-type basis for molecular-orbital studies of organic molecules. *J. Chem. Phys. 54*, 724−728.
(36) Rozas, I., Alkorta, I., and Elguero, J. (1998) Bifurcated hydrogen bonds: Three-centered interactions. *J. Phys. Chem. A 102*, 9925−9932.
(37) McGaughey, G. B., Gagne, M., and Rappe, A. K. (1998) π-stacking interactions: Alive and well in proteins. *J. Biol. Chem. 273*, 15458−15463.

DOI: 10.1021/acs.biochem.5b00195
Biochemistry 2015, 54, 4226−4235